Power Factors of *p*-type Half-Heusler Alloys ScNiBi, YNiBi, and LuNiBi by *ab initio* Calculations

M.J. Winiarski[a,*] and K. Bilińska[b]

[a] *Institute of Low Temperature and Structure Research, Polish Academy of Sciences, Okólna 2, 50-422 Wrocław, Poland*
[b] *Institute of Theoretical Physics, University of Wrocław, Pl. M. Borna 9, 50-204 Wrocław, Poland*

Received: 09.04.2020 & Accepted: 02.07.2020

Doi: 10.12693/APhysPolA.138.533 *e-mail: m.winiarski@int.pan.wroc.pl

Electronic structures and transport properties of RENiBi materials, where RE is Sc,Y, and Lu, were investigated with the density functional theory methods. The results of the Seebeck coefficient, electrical conductivity, and power factor obtained for YNiBi are in good accordance with available experimental data. The effective masses of hole-like carriers in RENiBi compounds are expected to be relatively low (0.24–0.36), and decrease with an increasing atomic number of the RE component. The longest relaxation time of carriers, estimated within the deformation potential theory, is expected for LuNiBi. However, this material revealed the narrower band gap, which limits the thermoelectric performance. Although the room temperature power factor reaching 2.5 mW/(K^2 m), obtained for optimally *p*-doped LuNiBi, is lower than the recent predictions for YNiSb and LuNiSb, the results presented in this work may encourage further experimental efforts in band engineering for Bi-based half-Heusler thermoelectric materials.

topics: bisimides, thermoelectric properties, electronic structure, calculation

1. Introduction

Global environmental policy related to climate change draws attention to energy conservation. Thermoelectric materials are investigated due to their possible applications in future devices for recovery of large amount of heat energy, e.g., the waste-heat in heavy industry. Recent advances in high-performance bulk thermoelectric materials [1–4] imply half-Heusler alloys as a promising family of compounds which may reveal improved thermoelectric power factor (PF) and figure of merit (ZT). Among the *d*-electron half-Heusler systems, the *p*-type Fe–Nb–Sb materials exhibit very high figure of merit [5–10].

Despite the fact that the experimental studies of thermoelectric properties of Ni-based phases, i.e., antimonides RENiSb [11–19], where RE is rare-earth element, indicate relatively low ZT at 300 K, the recent theoretical investigations suggest promising upper limits of PF for optimally doped *p*-type RENiSb intermetallics [20, 21]. Namely, PF in YNiSb and LuNiSb reaches 4–5 mW/(K^2 m) at room temperature. One may notice an increase in PF in this family of compounds with increasing atomic mass of RE ion. It is also worth recalling that the substitution of Sb with Bi ions leads to significant improvement of thermoelectric conversion efficiency in ZrCoSb [22].

Among the RENiBi half-Heusler phases PF of 1.3 mW/(K^2 m) (not optimized with a doping) was reported for YNiBi in the single experimental study [23]. The thermoelectric performance of *p*-type ScNiBi and YNiBi was also investigated in a semi-classical *ab initio* manner [24]. However, the data reported for these systems are somehow biased [25–27], because the results of calculations with standard exchange-correlation functionals yield underestimated band gaps of semiconductors. Furthermore, strong spin–orbit coupling in such heavy-band systems leads to substantial changes of valence bands and significant overestimation of power factors in the *p*-type regime [28].

The simple approximation of the constant relaxation time is generally unsuitable for theoretical predictions of PF for half-Heusler antimonides [20, 21]. The most challenging issue is therefore a reasonable approximation of the relaxation time of carriers. Quantitative predictions of PF may be based on an estimation of the relaxation time within the deformation potential theory [29]. In such a case, the scattering of charge carriers at high temperatures is dominated by acoustic phonons. Results based on this estimation were reported in numerous recent investigations of thermoelectric performance of various half-Heusler phases [30–36].

In this work, the electronic structures and thermoelectric properties of ScNiBi, YNiBi, and LuNiBi were studied from first principles. The fully relativistic band structures of these systems were obtained with the modified Becke–Johnson potential (MBJLDA [37]) and the standard LDA [38] approaches. The thermoelectric characteristics were obtained using the BolzTraP code [24]. The carrier relaxation time was approximated based on the deformation potential theory. The results of PF for the RENiBi materials were presented as a function of carrier concentration and temperature. Optimal PF predicted here may be assumed as reference upper limits for thermolectric performance in ScNiBi, YNiBi, and LuNiBi half-Heusler phases.

2. Computational details

Structural and elastic properties of RENiBi materials have been studied with the use of the Abinit package [39, 40]. The equilibrium geometries of the unit cells were found via stresses/forces relaxation. The elastic constants were obtained withing the density-functional perturbation theory. The projector augmented-wave (PAW) atomic datasets taken from the JTH table [41] with the Perdew–Wang [38] (LDA) parametrization of the exchange-correlation energy were employed for this task.

Next, the electronic structures of the systems studied were investigated using the full-potential linearized augmented planewave (FLAPW) method implemented in the Wien2k package [42]. The Perdew–Wang (LDA) [38] and MBJLDA [37] exchange-correlation functionals were used. The spin–orbit coupling was included and the $RK_{\max} = 8$ was used in all calculations. A $12 \times 12 \times 12$ $\boldsymbol{k}$-point mesh was employed for self-consistent calculations, whereas a 200000 $\boldsymbol{k}$-point mesh was required for calculations of the thermoelectric characteristics using the BolzTraP code [24]. The relaxation time of hole-like carriers was approximated within the deformation potential theory [29]. The details of this approach were extensively described in previous works [20, 21].

3. Results and discussion

The cubic lattice parameters a of 6.101, 6.328, and 6.251 Å, calculated here for ScNiBi, YNiBi, and LuNiBi, respectively, are slightly smaller with respect to the experimental data [23, 43, 44]. An underestimation of lattice parameters is a well-known feature of the LDA approach. A higher value of a for ScNiBi was reported in the recent GGA-based investigations [27]. The cubic lattice parameters of RENiBi systems are slightly bigger than those of corresponding RENiSb half-Heusler alloys [11, 13].

The total DOS and the partial DOS plots, obtained for RENiBi phases within the MBJLDA approach, are presented in Fig. 1. The relatively flat shapes of the total DOS below VBM indicate rather

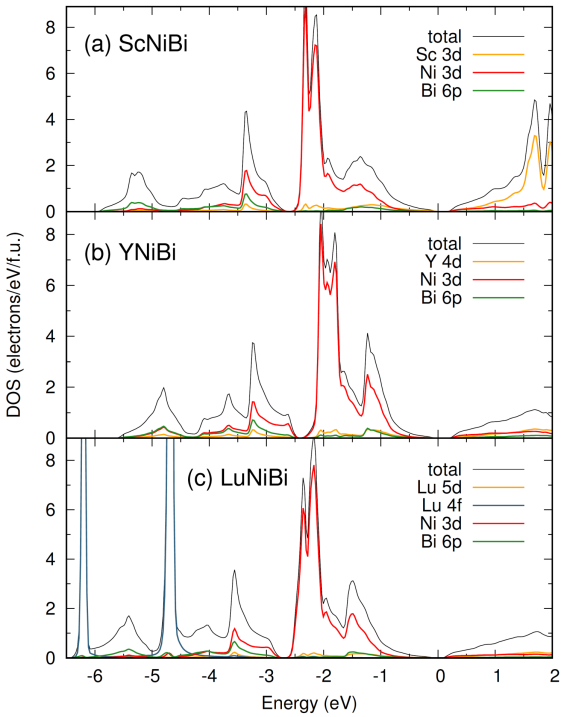

Fig. 1. Total density of states (DOS) and partial DOS contributions for (a) ScNiBi, (b) YNiBi, and (c) LuNiBi, calculated within the MBJLDA approach.

low effective masses of hole carriers in the materials studied. The valence band regions of these systems are dominated by the Ni $3d$ states hybridized with the Bi $6p$ states, whereas the RE d-type states are dominating in the conduction band region. The total DOS and the partial DOS contributions coming from Ni ions reveal similar overall shapes to those recently reported for RENiSb materials [20, 21].

As depicted in Fig. 1c, the two-folded peak of the Lu $4f$ states in LuNiBi is located below the Ni $3d$ bands. The binding energy of the Lu $4f$ states in LuNiBi is slightly higher than that of LuNiSb [21]. Furthermore, the positions of f-type DOS peaks in some LuNiSi and LuNiGe materials [45, 46], as well as LuN semiconductor [47], are closer to their Fermi level or VBM.

As gathered in Table I, the RENiBi phases are narrow band gap (E_g) semiconductors, similarly to the RENiSb materials [20, 21]. The values of LDA/MBLDA-derived E_g for the Bi-based compounds, which are below 0.19 eV, are significantly lower than those of the analogue antimonides. Furthermore, the experimental value of E_g for ScNiBi single crystal, estimated from the temperature dependence of the electrical resistivity to about 0.084 eV [43], is lower, whereas the experimental value of $E_g = 0.121$ eV for LuNiBi [48] is higher than our DFT-based predictions. It is also worth mentioning that the values of E_g^{MBJLDA} calculated for half-Heusler systems are generally close to the corresponding LDA/GGA results [20, 21].

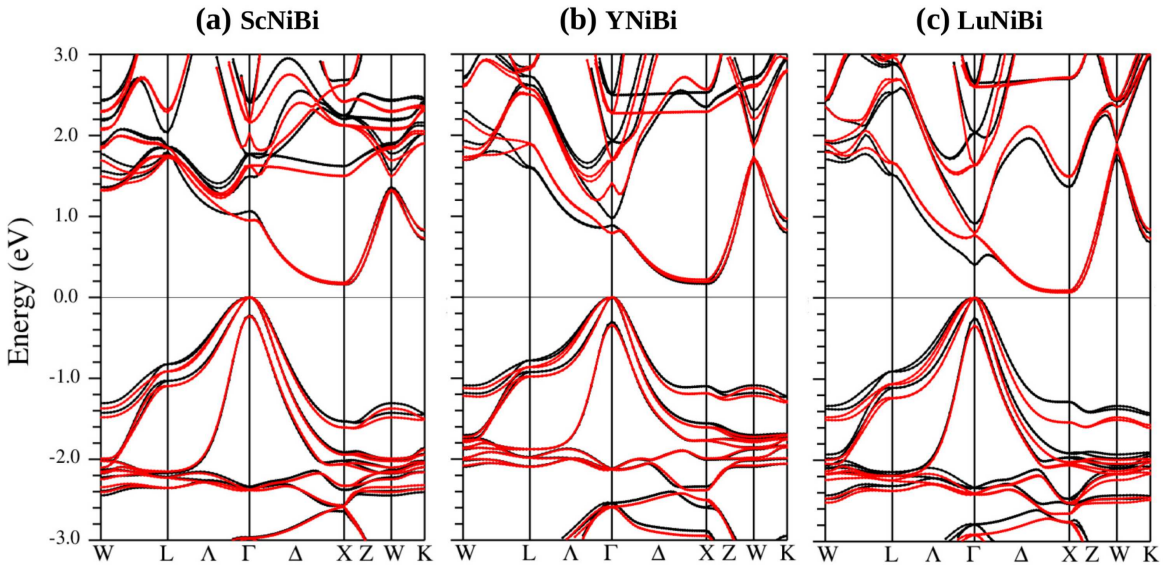

Fig. 2. Band structures of (a) ScNiBi, (b) YNiBi, and (c) LuNiBi, calculated within the LDA (black lines) and MBJLDA (red lines) approaches.

TABLE I

Band gaps E_g and heavy- and light-hole split-off energies Δ_{SO} (in eV) calculated for ScNiBi, YNiBi, and LuNiBi within the LDA and MBJLDA approaches.

Compound	E_g^{LDA}	$\Delta_{\mathrm{SO}}^{\mathrm{LDA}}$	E_g^{MBJLDA}	$\Delta_{\mathrm{SO}}^{\mathrm{mbjLDJ}}$
ScNiBi	0.158	0.222	0.163	0.231
YNiBi	0.166	0.304	0.190	0.345
LuNiBi	0.078	0.250	0.066	0.344

For some systems, i.e., LuNiBi, the use of the MBJLDA potential surprisingly leads to a small decrease in E_g with respect to E_g^{LDA}. The heavy- and light-hole split-off energies Δ_{SO}, which reveal the strong spin–orbit coupling in the bisimides, depend on a choice of an exchange–correlation functional. One may notice an increase in the MBJLDA-derived Δ_{SO} with increasing atomic number of the RE ion, which is an opposite effect to that characteristic of inverted band gap systems [49].

The band structures obtained for RENiBi phases, depicted in Fig. 2, are in good accordance with other theoretical results [3, 48, 50, 51]. The overall shapes of VBM and conduction band minimum (CBM) regions in all materials studied are similar to each other as well as those of RENiSb systems [20, 21]. The MBJ-derived modifications of band structures of RENiBi compounds are pronounced in energy regions distant from VBM and CBM. As mentioned above regarding the DOS plots in Fig. 1, the shapes of heavy- and light-hole bands in the RENiBi systems suggest rather low effective masses of the p-type carriers, which is generally desirable for the thermoelectric performance because of a high mobility of carriers [52].However, a flattened shape of CBM in these materials reveals rather high effective masses, which indicate low thermoelectric performance in the n-type regime.

The DFT-derived data required for an approximation of the relaxation time of hole carriers for RENiBi phases are presented in Table II. Despite the fact that the elastic constants C_β and deformation potentials E_β reveal small variations among these systems, the effective mass of hole carriers m_{eff} follows a clear trend on the atomic number of RE ions. Interestingly, the same values of m_{eff} were reported for corresponding ScNiSb and YNiSb phases, whereas LuNiSb was expected to exhibit slightly higher m_{eff} than that obtained here for LuNiBi [20, 21]. Such low effective masses of the p-type carriers were also reported for LaPtSb [30] and NbFeSb [32]. The values of C_β of RENiBi materials are generally higher than those of their Sb-based counterparts, which strongly affects the resulting relaxation time of the p-type carriers. Namely, the τ^{LDA} and τ^{MBJLDA} estimated for the RENiBi phases are significantly lower than those of the corresponding RENiSb half-Heusler alloys.

TABLE II

Elastic constants C_β (LDA), deformation potentials E_β for VBM, density of states effective masses m_{eff} of hole carriers, and relaxation times τ calculated for ScNiBi, YNiBi, and LuNiBi within the LDA and MBJLDA approaches.

	Compound		
	ScNiBi	YNiBi	LuNiBi
C_β [GPa]	199	199	206
E_β^{LDA} [eV]	39.7	36.8	36.7
$E_\beta^{\mathrm{MBJLDA}}$ [eV]	42.7	39.7	39.9
$m_{\mathrm{eff}}^{\mathrm{LDA}}$	0.36	0.27	0.24
$m_{\mathrm{eff}}^{\mathrm{MBJLDA}}$	0.36	0.27	0.22
τ^{LDA} [fs]	20.3	36.4	45.2
τ^{MBJLDA} [fs]	17.6	31.3	43.6

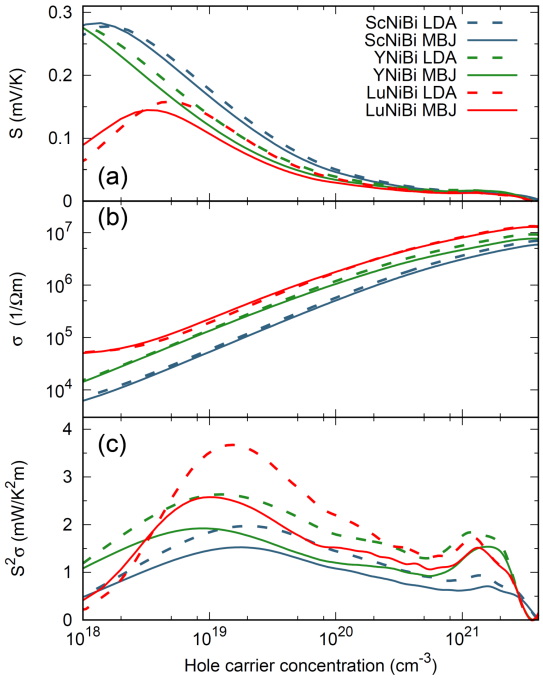

Fig. 3. (a) Seebeck coefficient S, (b) electrical conductivity σ, and (c) power factor $S^2\sigma$ at 300 K, calculated for hole-doped ScNiBi, YNiBi, and LuNiBi within the MBJLDA (solid lines) and LDA (dotted lines) approaches.

The results of the Seebeck coefficient S, electrical conductivity σ, and power factor PF $= S^2\sigma$ as a function of the carrier concentration p at 300 K, obtained for the RENiBi phases, are presented in Fig. 3. The variation of the features of band structures, discussed above for the data gathered in Table I, leads to different results of the LDA and MBJLDA calculations.

The dependences of $S(p)$ obtained for ScNiBi and YNiBi are similar to each other. Maximum values of $S(p)$ in the materials reveal for small p, and diminish with increasing p. In the Lu-bearing system, $S(p)$ is strongly suppressed by the narrow band gap. At the same time, σ of this system is significantly higher than those of the Sc- and Y-bearing phases, which is directly related to the highest relaxation time τ predicted for the Lu-based bisimide. Because the final results of PF are dominated by σ, the superior thermoelectric performance is obtained for LuNiBi. On one hand, PF of RENiBi phases is connected with atomic numbers of RE ions, which are revealed in very low effective masses of the p-type carriers. On the other hand, the relatively narrow band gaps in these systems limit their thermoelectric performance with respect to that of RENiSb half-Heusler alloys [20, 21]. One may further consider that the PF of LuNiBi may be significantly improved by a widening of a band gap, as demonstrated in the case of high performance p-type FeNbSb based thermoelectric materials [9].

According to the experimental study for the YNiBi phase [23], this material exhibits small values of S (below 0.1 mV/K) and σ ($10^5\ \Omega^{-1}\ \mathrm{m}^{-1}$) for carrier concentration p of 10^{19} cm^{-3} at room temperature, which are in good accord with the theoretical predictions presented in Fig. 3. However, the experimental PF of 1.1 mW/(K^2 m) at 300 K is noticeably lower than the maximum theoretical value of 1.8 mW/(K^2 m). One may consider that the electronic structures and scattering of carriers of real systems are strongly affected by various defects, which are not included in the calculations for ideal crystals. Nevertheless, the results of σ presented here are reasonable. It should be mentioned that slight overestimations of predicted σ in a low T-range and satisfactory accordance between measured and calculated σ in a high-T regime, were reported for ScNiSb [16, 20] and FeNbSb materials [32]. The theoretical results may be generally regarded as the upper limits of PF possible to obtain in real materials. The power factors of RENiBi compounds at 300 K, presented in Fig. 3, are lower than those predicted for YNiSb and LuNiSb [21] and the literature data for the best known p-type thermoelectric materials [53].

The experimental thermal conductivity $\kappa = 3.5$ W/(m K), reported for YNiBi [23], is significantly lower than the previous theoretical estimation of 10.6 W/(m K) [54]. The room temperature figure of merit in YNiBi, being less than 0.08, is comparable with those reported for RENiSb systems [11–19]. According to the theoretical predictions for ScNiBi, YNiBi, and LaNiBi [54], κ decreases with increasing atomic number of RE ions in the RENiBi family of compounds. Thus, the superior figure of merit in the Lu-bearing phase can be expected. This issue requires further experimental research.

The dependences of the optimal PF values on the temperature for the RENiBi materials, displayed in Fig. 4, are rather flat regardless the carrier concentration. The LDA-derived optimal PF are clearly higher than the results obtained within the modified Becke–Johnson approach. However, the latter parametrization of the exchange-correlation energy yields more reasonable band structures of semiconductors [37], and one may assume that the MBJLDA-derived data are better predictions of the properties of real systems.

As can be inferred from the temperature dependences of the power factor of RENiBi phases with different concentrations of hole carriers, depicted in Fig. 5, the best thermoelectric performance of these systems at room temperature is predicted for p of about 10^{19} cm^{-3}. The optimal doping of about 10^{20} cm^{-3} is predicted for the higher temperature regime. Despite the fact that the dependences of PF on T in these materials are slightly different from those previously reported for Ni- and Pd-based antimonides [20, 21], i.e, the small variation of optimal PF on T is found for the bisimides, the optimal

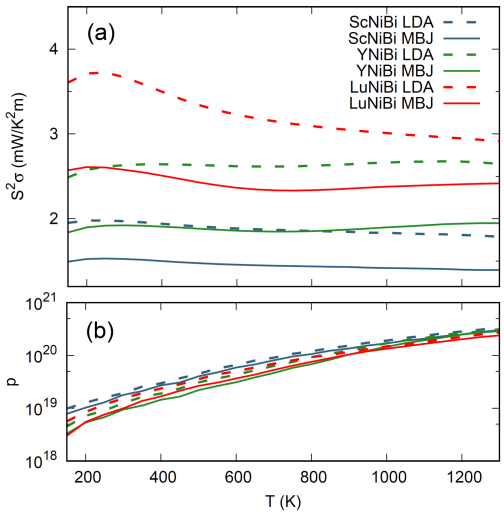

Fig. 4. (a) Optimal power factor $S^2\sigma$ in a wide range of temperature and (b) corresponding hole carrier concentration p, calculated for ScNiBi, YNiBi, and LuNiBi, within the LDA (dotted lines) and MBJLDA (solid lines) approaches.

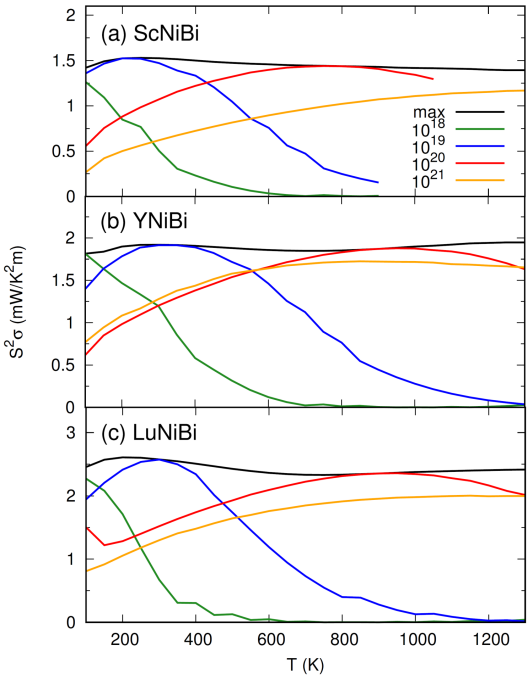

Fig. 5. Power factors $S^2\sigma$ for various hole carrier concentrations (in cm^{-3}) for (a) ScNiBi, (b) YNiBi, and (c) LuNiBi, calculated within the MBJLDA approach. The optimal PF curve (labeled max) corresponds to optimal carrier concentration, which generally varies with changing the temperature.

doping levels at room temperature, as well as at higher temperatures, seem common for RENiSb and RENiBi half-Heusler alloys. The origin of the relatively high PF in Ni-based phases at low temperatures is connected with the numerous split bands below VBM and low effective masses of hole carriers, which promote a high Seebeck coefficient and a high relaxation time of the p-type carriers.

4. Conclusions

The electronic structures of ScNiBi, YNiBi, and LuNiBi exhibit features that promote an occurrence of high thermoelectric power factors. Although these systems show the lowest effective masses of the p-type carriers among the Ni-based half-Heusler bisimides and antimonides, the very narrow band gaps of the Bi-bearing half-Heusler alloys limit their thermoelectric performance with respect to those of similar antimonides. The power factor at room temperature predicted here for LuNiBi, reaching 2.5 mW/(K^2 m) for carrier concentrations of about 10^{19} cm^{-3}, might be improved with some band engineering. The results presented in this work may encourage further experimental investigations of electronic structures and thermoelectric properties of RE element bearing half-Heusler bisimides.

References

[1] X. Shi, L. Chen, C. Uher, *Int. Mater. Rev.* **61**, 379 (2016).

[2] S. Chen, Z. Ren, *Mater. Today* **16**, 387 (2013).

[3] J.-W.G. Bos, R.A. Downie, *J. Phys. Condens. Matter* **26**, 433201 (2014).

[4] T. Zhu, C. Fu, H. Xie, Y. Liu, X. Zhao, *Adv. Energy Mater.* **5**, 1500588 (2015).

[5] C. Fu, S. Bai, Y. Liu, Y. Tang, L. Chen, X. Zhao, T. Zhu, *Nat. Commun.* **6**, 8144 (2015).

[6] A. Tavassoli, F. Failamani, A. Grytsiv, G. Rogl, P. Heinrich, H. Müller, E. Bauer, M. Zehetbauer, P. Rogl, *Acta Mater.* **135**, 263 (2017).

[7] D.P. Young, P. Khalifah, R.J. Cava, A.P. Ramirez, *J. Appl. Phys.* **87**, 317 (2000).

[8] G. Joshi, R. He, M. Engber, G. Samsonidze, T. Pantha, E. Dahal, K. Dahal, J. Yang, Y. Lan, B. Kozinsky, Z. Ren, *Energy Environ. Sci.* **7**, 4070 (2014).

[9] C. Fu, T. Zhu, Y. Liu, H. Xie, X. Zhao, *Energy Environ. Sci.* **8**, 216 (2015).

[10] R. He, D. Kraemer, J. Mao et al., *Proc. Natl. Acad. Sci. USA* **113**, 13576 (2016).

[11] J. Oestreich, U. Probst, F. Richardt, E. Bucher, *J. Phys. Condens. Matter* **15**, 635 (2003).

[12] K. Kawano, K. Kurosaki, H. Muta, S. Yamanaka, *J. Appl. Phys.* **104**, 013714 (2008).

[13] V.V. Romaka, L. Romaka, A. Horyn, P. Rogl, Y. Stadnyk, N. Melnychenko, M. Orlovskyy, V. Krayovskyy, *J. Solid State Chem.* **239**, 145 (2016).

[14] K. Synoradzki, K. Ciesielski, L. Kępiński, D. Kaczorowski, *J. Appl. Phys.* **123**, 235101 (2018).

[15] K. Synoradzki, K. Ciesielski, L. Kępiński, D. Kaczorowski, *Phys. B* **536**, 659 (2018).

[16] I. Wolańska, K. Synoradzki, K. Ciesielski, K. Załęski, P. Skokowski, D. Kaczorowski, *Mater. Chem. Phys.* **227**, 29 (2019).

[17] K. Synoradzki, K. Ciesielski, I. Veremchuk, H. Borrmann, P. Skokowski, D. Szymański, Y. Grin, D. Kaczorowski, *Materials* **12**, 1723 (2019).

[18] I. Wolańska, K. Synoradzki, K. Ciesielski, K. Załęski, P. Skokowski, D. Kaczorowski, *Mater. Chem. Phys.* **227**, 29 (2019).

[19] K. Ciesielski, K. Synoradzki, I. Wolańska, P. Stachowiak, L. Kępiński, A. Jeżowski, T. Toliński, D. Kaczorowski, *J. Alloys Compd.* **816**, 152596 (2019).

[20] M.J. Winiarski, K. Bilińska, K. Ciesielski, D. Kaczorowski, *J. Alloys Compd.* **762** 901 (2018).

[21] M.J. Winiarski, K. Bilińska, *Intermetallics* **108**, 55 (2019).

[22] H. Zhu, R. He, J. Mao et al., *Nat. Commun.* **9**, 2497 (2018).

[23] S. Li, H. Zhao, D. Li, S. Jin, L. Gu, *J. Appl. Phys.* **117** 205101 (2015).

[24] G.K.H. Madsen, D.J. Singh, *Comput. Phys. Commun.* **175**, 67 (2006).

[25] J. Yang, H. Li, T. Wu, W. Zhang, L. Chen, J. Yang, *Adv. Funct. Mater.* **18**, 2880 (2008).

[26] S. Sharma, P. Kumar, *Mater. Res. Express.* **5**, 046528 (2018).

[27] A. Bano, M.G. Gaur, *Mater. Res. Express.* **6**, 056516 (2019).

[28] S.-D. Guo, *J. Alloys Compd.* **663**, 128 (2016).

[29] J. Bardeen, W. Shockley, *Phys. Rev.* **80**, 72 (1950).

[30] Q.Y. Xue, H.J. Liu, D.D. Fan, L. Cheng, B.Y. Zhao, J. Shi, *Phys. Chem. Chem. Phys.* **18** 17912 (2016).

[31] O.M. Abid, S. Menouer, A. Yakoubi, H. Khachai, S. Bin Omran, G. Murtaza, D. Prakash, R. Khenata, K.D. Verma, *Superlatt. Microstruct.* **93**, 171 (2016).

[32] A.J. Hong, L. Li, R. He, J.J. Gong, Z.B. Yan, K.F. Wang, J.-M. Liu, Z.F. Ren, *Sci. Rep.* **6**, 22778 (2016).

[33] T. Fang, S. Zheng, H. Chen, H. Cheng, L. Wang, P. Zhang, *RSC Adv.* **6**, 10507 (2016).

[34] T. Fang, S. Zheng, T. Zhou, L. Yan, P. Zhang, *Phys. Chem. Chem. Phys.* **19**, 4411 (2017).

[35] K. Kaur, R. Kumar, *J. Alloys Compd.* **727**, 1171 (2017).

[36] K. Kaur, R. Kumar, D.P. Rai, *J. Alloys Compd.* **763**, 1018 (2018).

[37] F. Tran, P. Blaha, *Phys. Rev. Lett.* **102**, 226401 (2009).

[38] J.P. Perdew, Y. Wang, *Phys. Rev. B* **45**, 13244 (1992).

[39] X. Gonze, J.-M. Beuken, R. Caracas et al., *Comput. Mater. Sci.* **25**, 478 (2002).

[40] X. Gonze, B. Amadon, P.-M. Anglade et al., *Comput. Phys. Commun.* **180**, 2582 (2009).

[41] F. Jollet, M. Torrent, N. Holzwarth, *Comput. Phys. Commun.* **185**, 1246 (2014).

[42] P. Blaha, K. Schwarz, P. Sorantin, S.B. Trickey, *Comput. Phys. Commun.* **59**, 399 (1990).

[43] L. Deng, Z.H. Liu, X.Q. Ma, Z.P. Hou, E.K. Liu, X.K. Xi, W.H. Wang, G.H. Wu, X.X. Zhang, *J. Appl. Phys.* **121**, 105106 (2017).

[44] J. Chen, H. Li, B. Ding, Z. Hou, E. Liu, X. Xia, H. Zhang, G. Wu, W. Wang, *J. Alloys Compd.* **784**, 822 (2019).

[45] M. Samsel-Czekała, M.J. Winiarski, *Intermetallics* **20**, 63 (2012).

[46] J.R. Salvador, J.R. Gour, D. Bilc, S.D. Mahanti, M.G. Kanatzidis, *Inorg. Chem.* **43**, 1403 (2004).

[47] M.J. Winiarski, D. Kowalska, *Mater. Res. Express* **6**, 095910 (2019).

[48] F. Casper, C. Felser, *Z. Anorg. Allg. Chem.* **634**, 2418 (2008).

[49] M.J. Winiarski, P. Scharoch, M.P. Polak, *J. Alloys Compd.* **613**, 33 (2014).

[50] P. Larson, S.D. Mahanti, S. Sportouch, M.G. Kanatzidis, *Phys. Rev. B* **59**, 15660 (1999).

[51] M. Narimani, Z. Nourbakhsh, *Thin Solid Films* **634**, 112 (2017).

[52] Y. Pei, H. Wang, G.J. Snyder, *Adv. Mater.* **24**, 6125 (2012).

[53] D. Zhao, G. Tan, S. Hao et al., *Science* **351**, 141 (2016).

[54] J. Carrete, W. Li, N. Mingo, S. Wang, S. Curtarolo, *Phys. Rev. X* **4**, 011019 (2014).